IEEE Access
Multidisciplinary | Rapid Review | Open Access Journal

Received January 25, 2022, accepted February 6, 2022, date of publication February 9, 2022, date of current version February 17, 2022.

Digital Object Identifier 10.1109/ACCESS.2022.3150310

Estimation of the Frequency-Dependent Parameters of Transmission Lines by Using Synchronized Measurements

CASSIO GEREZ[1], EDUARDO WERLEY S. ÂNGELOS[2], (Member, IEEE), FELIPE P. ALBUQUERQUE[1], EDUARDO C. MARQUES DA COSTA[1], ALFEU J. SGUAREZI FILHO[3], (Senior Member, IEEE), AND LUISA H. BARTOCCI LIBONI[4], (Member, IEEE)

[1]Polytechnic School, University of São Paulo (EPUSP), São Paulo 05508-010, Brazil
[2]Research, Innovation and Dissemination Center for Neuromathematics (NeuroMat), University of São Paulo (USP), São Paulo 05508-060, Brazil
[3]Center for Engineering, Modeling and Applied Social Sciences, Federal University of ABC (UFABC), Santo André 09210-580, Brazil
[4]Federal Institute of Education Science and Technology of São Paulo (IFSP), Sertãozinho 14801-600, Brazil

Corresponding author: Cassio Gerez (cassio.gerez@usp.br)

This work was supported in part by the Coordenação de Aperfeiçoamento de Pessoal de Nível Superior (CAPES), National Counsel of Scientific and Technological Research (CNPq), under Grant 142049/2018-2; and in part by the São Paulo Research Foundation (FAPESP) under Grant 19/05381-9 and Grant 21/01325-7.

ABSTRACT Transmission line parameters are usually calculated based on technical and environmental approximations, e.g. line height, cable conductivity, etc. These characteristics vary depending on the environment and technical issues, meaning that the transmission line should be considered as a dynamic system with time-varying parameters. Estimation methods are a useful way to determine line parameters taken into account such characteristics. Most methods estimate these parameters at 50 $\sim$ 60 Hz, useful for steady state analysis. However, for transient state or harmonic distortion analyses, a frequency range should be estimated, which varies according to the phenomenon to be investigated. In this matter, considering the gap existent of studies to estimate frequency-dependent parameters, we propose an efficacious and simplified method based on the two-port line representation and the well-known least squares method to estimate these parameters of a transmission line with 400 km length, considering a minimum number of synchronized measurements from 1 Hz up to 250 Hz.

INDEX TERMS Frequency-dependent parameters, parameter estimation, synchronized measurements, transmission lines.

NOMENCLATURE

$Z_{ext_{ii}}$	self external impedance.
$Z_{ext_{ik}}$	mutual external impedance.
ΔZ_{ii}	self earth-return impedance (Carson term).
ΔZ_{ik}	mutual earth-return impedance (Carson term).
Z_{skin}	impedance due to skin effect (internal impedance).
r_i	radium of the wires (or the geometric mean radius - GMR).
h_i	height between the wires and the ground.
μ_0	magnetic permeability.
d_{ik}	distance between conductor i and k.
$D_{ik'}$	distance between conductor i and the image k'.
σ_g	soil conductivity.
h_k	height of the wire k from the ground.
V_s	voltage at the sending end.
V_r	voltage at the receiving end.
I_s	current at the sending end.
I_r	current at the receiving end.
A, B, C, D	two-port network terms.
l	line length.
γ	propagation function of the line.
Z	impedance of the line.
Y	admittance of the line.
$Z(s)$	frequency-dependent impedance.
s	complex frequency.
A_{tf}	numerator of the transfer function.

The associate editor coordinating the review of this manuscript and approving it for publication was Youngjin Kim.

B_{tf}	denominator of the transfer function.
a_n	n coefficient of A_{tf}.
b_m	m coefficient of B_{tf}.
$R(\omega)$	resistance of the line dependent of frequency ω.
$L(\omega)$	inductance of the line dependent of frequency ω.
$\boldsymbol{z}$	complex vector of size M ($M \geq n+m+1$).
$\boldsymbol{H_z}$	Jacobian Matrix of size $M \times n+m+1$.
$\boldsymbol{x}$	complex vector with the state variables.
$J(\hat{x})$	performance index.
$\hat{\boldsymbol{x}}$	vector that minimizes the performance index.
$\boldsymbol{Q}$	matrix with the same dimensions of $\boldsymbol{H_z}$.
$\boldsymbol{R}$	upper triangular matrix representing the reduced version of the factorization.
$\boldsymbol{W}$	weight matrix related to measurements.
$\boldsymbol{K}$	estimator gain matrix.
$\boldsymbol{P}$	estimation error covariance.
$\boldsymbol{R}$	variance of the noise corrupting the signal.
Z_{eq}	equivalent impedance of a long line.
Y_{eq}	equivalent admittance of a long line.
Z_c	characteristic impedance of a line.
Y_c	characteristic admittance of a line.

I. INTRODUCTION

The previous knowledge of the series impedance and shunt admittance of transmission lines is required for the reliable operation of an entire power system, specially considering the increasing context of smart grid networks [1], [2]. The correct parameterization of relays, fault detection/location, propagation characteristics, surge protection are directly dependent on the accuracy in which the line parameters are determined.

The frequency-dependent parameters of transmission lines are usually calculated based on the physical and structural characteristics of the line (line height, geometry of the towers, bundle, cables, and soil characteristics) while considering the earth-return current and the skin effect in the wires. The classical analytic method for parameters calculation is based on the Bessel and Carson formulation, which leads to certain inaccuracies because of improper approach on the soil conductivity and geometrical structure of the lines [3], [4]. In general, soil resistivity varies from 10 up to 10.000 Ωm; depending on moisture, composition, and temperature. However, it is well known that such characteristics are affected by the different environmental conditions and also along the terrain in which the line cross through [5], [6]. Furthermore, the transmission line is subject to several technical issues, such as: unbalanced bundles, different aging through the line sections, degradation of tower insulators, and various others. In this sense, it is possible to state that the line may be considered as a dynamic system with time-varying parameters.

Introduced in the 70's and developed since then [7]–[9], the transmission line parameters estimation (TLPE) represents an accurate procedure to determine these electrical parameters by using synchronized current and voltage measurements at both terminals of the line. With the advent of modern monitoring and measurement technologies, and state of the art in estimation methods, several TLPE methods have been proposed since 2000's, with several contributions to the development of new state estimation methods and transmission line models [10]–[15].

Some TLPE methods have taken place in the last decade in which dynamical equations are used to model measurements of transmission lines. In some cases, the parameter estimation is carried out in the time domain by employing synchronized current and voltage measurements during transient state at both sending and receiving terminals [16], [17]. Despite these methods show a good performance, the parameters estimation is only possible after transient occurrences (fault, abrupt load varying, lightning etc). On the other hand, there are also estimation methods that are developed in the frequency domain by using phasor measurements at both ends of the line [18]–[21]. Some phasorial methods propose the estimators by using equations based on the well-known π line model and the Gauss-Newton method for non-linear equations [12], [22]. These methods can be applied from steady state measurements, representing a notable advantage compared to those methods restricted only to transient state, in which the parameters estimation can be only possible after a transient or fault occurrences [15].

A summary of papers and studies that dealt with TLPE in the last two decades is presented in Table 1.

Although various transient- and steady-state TLPE methods show to be accurate in specific operation and technical conditions, none of them take into consideration the frequency dependency of the estimated series parameters, i.e. longitudinal resistance and inductance, as seen in Table 1. The majority of papers that discuss frequency-dependent parameters focuses only on the model itself or in the analysis of systems in such conditions and not the TLPE. Indeed, this proposal represents a very complex task, since most of time-domain line models are developed by using fitting techniques, and TLPE methods have been developed for specific analyses at fundamental frequency of 50 or 60 Hz [35]–[37].

The importance of taking the frequency-dependent nature of these parameters in consideration has been treated in the literature for a long time, as in some transient cases, the treatment of the parameters as constant can produce a magnification of the high harmonics of the signals and, consequently, generate distortions in the shapes and magnitudes of waves. Also, parameters of transmission lines with ground return, as well as the inner impedance of a conductor are highly dependent of the frequency range [38].

In this context, this paper proposed an original and simplified method to calculate and estimate frequency dependent series parameters of a transmission line TL with 400 km length. Focusing on the TLPE of these frequency dependent parameters is the major novelty of the presented study, as literature review shown that such approach is nonexistent. The approach considers that current, power and voltage

TABLE 1. Summary of TLPE publications and papers from the last 20 years.

Reference	Year	Focus of the paper
[10]	1999	TLPE at fundamental frequency via LS for transmission line remote protection
[23]	2001	TLPE at fundamental frequency via Generalized Equation Error
[24]	2003	TLPE at fundamental frequency together with fault/detection location technique
[12]	2008	TLPE at fundamental frequency via Newton-Raphson algorithms using measurements at both ends
[22]	2008	TLPE at fundamental frequency via Newton-Raphson algorithms using synchronized measurements at both ends
[16]	2009	TLPE at fundamental frequency via LS using re-synchronized measurements
[18]	2011	TLPE at fundamental frequency via Extended-Kalman Filter (EKF) using Phasor Measurement Units (PMU) measurements
[25]	2011	TLPE at fundamental frequency via an optimization model using long-term synchronized phasor measurements
[26]	2012	TLPE at fundamental frequency via LS for evaluation of the influence of different transmission line lengths
[27]	2013	TLPE at fundamental frequency via LS and Kirchoff's Law using PMU measurements
[28]	2014	TLPE at fundamental frequency via weighted least squares (WLS) and PMU measurements
[17]	2015	TLPE at fundamental frequency via LS considering a hybrid domain model (phase and modal) using synchronised fault records
[29]	2017	TLPE at fundamental frequency via Nonlinear Weighted Least Squares (NWLS) using two devices to acquire measurements, PMU and Supervisory Control and Data Acquisition (SCADA)
[19]	2017	TLPE at fundamental frequency via an optimization model solved through a derived Newton method
[30]	2018	TLPE at fundamental frequency via Cloud Computing using PMU and SCADA measurements
[13]	2018	TLPE at fundamental frequency via a M-estimator using PMU measurements
[31]	2019	TLPE at fundamental frequency via recursive least-squares (RLS) using one terminal data sampling
[32]	2020	TLPE at fundamental frequency via Kalman filter methods using synchronized measurements
[15]	2021	TLPE at fundamental frequency via two LS methods using synchronized measurements
[33]	2021	TLPE at fundamental frequency via an optimization model solved through Firefly Algorithm (FA)
[34]	2021	TLPE at fundamental frequency via an optimization model solved through Whale Optimization Algorithm (WOA) using voltage and current measurements

measurements are available at both ends of an overhead TL for a given frequency range (1∼250 Hz). Such measurements can be obtained through synchronized measurements via PSCAD simulations. In real cases, these values can be obtained through fault records by digital relays and subsequent frequency decomposition [39].

Since the frequency values are known, parameters are calculated by using the two-port equivalent line model in these fixed frequencies points. Finally, the coefficients that represent the transfer function (TF) of the parameters that are frequency-dependent are determined, initially, via five least-square (LS) methods, to represent the curves of frequency-dependent resistance and inductance into the established frequency range. In order to find the LS method that produces the best estimation and verify the influence of different values of voltage and loading in the proposed approach, the transmission line is modeled in the PSCAD under separate simulations considering different loading and voltage conditions. All the reference values were obtained from the transmission line and cable constants (TLCC) algorithm using the Deri-Semlyen model to calculate the ground impedance in PSCAD. The Deri-Semlyen method is the way that PSCAD TLCC algorithm approximates Carson's Integral in overhead transmission lines, which is responsible to determine the ground impedance. More of Deri-Semlyen can be found in [40]. The synchronized measurements are simulated and obtained from 38 frequency points, which are logarithmically distributed from 1 Hz up to 250 Hz (frequency range in which occurs most of switching and maneuver transients in power systems) [35]. The proposed method provides an efficient application for transient studies and harmonic distortion analysis up to the frequency where the parameters are estimated, helping to improve parameterization of protection and simulation of transmission systems when dealing with such phenomenons.

The main goals of the paper can be summarized as follows:

- Proposal of a simplified and efficient method for estimation of the frequency-dependent transmission line parameters;
- The use of a reduced number of measurements to estimate the frequency-dependent parameters of a TL with 400 km length;
- Estimation of a frequency range which represents most of switching and maneuvers electromagnetic transients phenomena in power transmission systems (1∼250 Hz).

The paper is structured as follows: Section II presents an overview on overhead TL parameters and models, Section III introduces the proposed method, Section IV presents the simulations, results and discussions. Finally, conclusions and further researches are presented in Section V. An Appendix describes the derivation of the main equations of the method.

II. OVERHEAD TRANSMISSION LINE PARAMETERS

There are several overhead TL models available in the technical literature. A well-established one is the π line model, which is composed of shunt admittance and series impedance parameters. Thus, a long transmission line can be modeled by a cascade of π equivalent circuits or as a hyperbolic approximation, i.e. the distributed nature of the line parameters are represented by lumped elements. The detailed description of such models, helps to understand how the frequency directly influence these parameters. Figure 1 shows a π equivalent circuit representing an overhead TL [12].

Although steady state representations are more common in TL modeling, some specific cases, such as transient and harmonic studies [17], should take into consideration the frequency effect on the line parameters. These are calculated based on the physical and geometrical characteristics of the conductor, being influenced by the environment (e.g. soil characteristics and temperature).

Several works in the literature consider that the shunt parameters (conductance and capacitance) are not frequency-dependent. Nevertheless, the parameters of the impedance (resistance and inductance) are frequency dependent due to the earth-return current and skin effect [17], [41].

The self and mutual impedance of two conductors i and k can be calculated as a function of the frequency by using the conventional Bessel formulation and Carson's terms. In this methodology, several approaches are considered, e.g. constant soil resistance, line height, air permittivity, and bundle characteristics. These approaches are far to be accurate and lead to errors in the overhead TL parameters determination [15], [39]. The self and mutual impedances can be calculated through equations 1 and 2, respectively [42].

$$Z_{ii}(\omega) = Z_{ext_{ii}}(\omega) + Z_{skin}(\omega) + \Delta Z_{ii}(\omega) \tag{1}$$

$$Z_{ik}(\omega) = Z_{ext_{ik}}(\omega) + \Delta Z_{ik}(\omega) \tag{2}$$

The parameters due to the skin effect are more expressive at low frequencies, while the soil effect is more preeminent at medium to high frequencies.

The self and mutual external impedances, which are represented by inductive reactances, considering the image method, can be obtained from equations 3 and 4 [42].

$$Z_{ext_{ii}} = j\omega\frac{\mu_0}{2\pi}\ln\frac{2h_i}{r_i} \tag{3}$$

$$Z_{ext_{ik}} = j\omega\frac{\mu_0}{2\pi}\ln\frac{D_{ik'}}{d_{ik}} \tag{4}$$

The external impedance values are given by a frequency dependent inductive reactance with a constant inductance, which is calculated as a function of the geometry, distances and physical characteristics of the medium.

The self and mutual earth-return impedance parameters are given by using Carson's formulation. It considers the calculation of the axial electric field in the ground and further obtainment of the magnetic field from Maxwell's curl equation. Considering some approximations, improper integrals are able to determine the self and mutual earth-return impedance as presented in equations 5 and 6.

$$\Delta Z_{ii}(\omega) = \frac{j\omega\mu_0}{\pi}\int_0^\infty \frac{e^{-2h_i u}}{\sqrt{u^2 + j\omega\mu_0\sigma_g} + u}du \tag{5}$$

$$\Delta Z_{ik}(\omega) = \frac{j\omega\mu_0}{\pi}\int_0^\infty \frac{e^{-2(h_i+h_k)u}\cos d_{ik}u}{\sqrt{u^2 + j\omega\mu_0\sigma_g} + u}du \tag{6}$$

To solve these integrals, the expansion by infinite series term is employed [3].

The parameter Z_{skin}, which results from the electromagnetic field inside the conductors, it is normally neglected in transmission line parameters studies dealing with voltages above 138 kV [4].

III. LINE MODELING AND FREQUENCY DEPENDENT TLPE

First, a transmission line with 400 km length is modeled for validation of the proposed TLPE method by means of current, power, and voltage measurements at both sending and receiving ends of the line. This way, the frequency-dependent parameters are previously known in order to simulate the measurements at the line terminals, and also are defined as a reference value to evaluate the estimated parameters. The initial proposal is to estimate the frequency-dependent parameters from 1 up to 250 Hz, a frequency range in which most of switching and maneuvers electromagnetic transients are included.

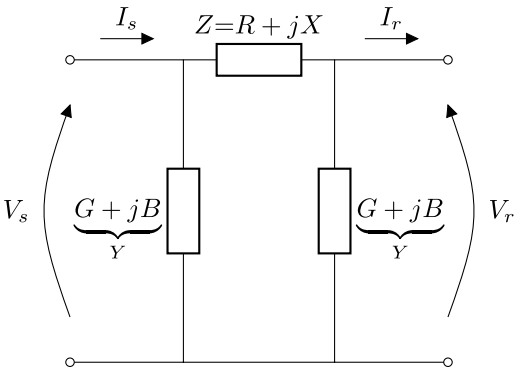

FIGURE 1. Overhead TL representation by a single π equivalent circuit.

Thus, assuming that it is possible to obtain the current and voltage measurements in the given range of frequencies at both ends of the line, it is also possible to determine the parameters by using the two-port network, which is represented by equations 7-10, based in the well known two-port model [43]. The derivation of equations 7-10 can be found in the Appendix.

$$A = \frac{V_s I_s + V_r I_r}{V_s I_r + V_r I_s} \tag{7}$$

$$B = \frac{V_s - AV_r}{I_r} \tag{8}$$

$$C = \frac{I_s - DI_r}{V_r} \tag{9}$$

$$D = A \tag{10}$$

Terms A, B, C and D are obtained from the impedance and admittance parameters of the transmission line.

From equations 7-10, the line parameters and propagation function can be obtained, as expressed in equations 11-13, based in the hyperbolic model [43].

$$\gamma^2 = \left(\frac{\cosh^{-1}A}{l}\right)^2 \tag{11}$$

$$\frac{B}{C} = \frac{Y}{Z} \tag{12}$$

$$ZY = \left(\frac{\cosh^{-1}A}{l}\right)^2 \tag{13}$$

As $\gamma = \sqrt{ZY}$ [43], equation 11 can be presented as 13. Hence, the value of Z, and consequently of R and L, can be calculated by replacing equation 12 in 13. The derivation of equations 11-13 can be found in the Appendix.

Several frequency-dependent TL models are developed directly in the time domain by using rational functions and

an equivalent electric circuit [41]. In these methods, a transfer function is determined to fit the frequency dependent parameters. This function will represent the parameters in the given frequency range. So, when using this function in a fixed frequency (e.g. 60 Hz) it will result in a real and imaginary part, which will represent respectively the resistance and inductance of the line in this frequency. One of these methods is known as the Levy approach, where the frequency-dependent TL impedance is fitted by equation 14 [44]. The impedance parameters are also frequency dependent, as shown in equation 15 [38].

$$Z(s) = \frac{a_0 + a_1 s + a_2 s^2 + \ldots + a_n s^n}{1 + b_1 s + b_2 s^2 + \ldots + b_m s^m} = \frac{A_{tf}(s)}{B_{tf}(s)} \quad (14)$$

$$Z(s) = R(\omega) + sL(\omega) \quad (15)$$

$$s = j\omega \quad (16)$$

Multiplying equation 14 by $B_{tf}(s)$ and rewriting as a function of one measurement $z_1(s) = R_1(\omega) + sL_1(\omega)$, equation 17 is found.

$$\begin{aligned} z_1(1 + b_1 s + b_2 s^2 + \ldots + b_m s^m) &= a_0 + a_1 s + a_2 s^2 + \ldots + a_n s^n \\ z_1 &= a_0 + a_1 s + a_2 s^2 + \ldots + a_n s^n - z_1 b_1 s_1 \\ &\quad - z_1 b_2 s_1^2 + \ldots z_1 b_m s_1^m \end{aligned} \quad (17)$$

Expanding the equation 17 to a series of k measurements, an equation system is obtained and expressed in matrix form as follows:

$$\begin{bmatrix} z_1 \\ z_2 \\ z_3 \\ \vdots \\ z_k \end{bmatrix} = \begin{bmatrix} 1 & s_1 & s_1^2 & \ldots & s_1^n & -z_1 s_1 & -z_1 s_1^2 & \ldots & -z_1 s_1^m \\ 1 & s_2 & s_2^2 & \ldots & s_2^n & -z_2 s_2 & -z_2 s_2^2 & \ldots & -z_2 s_2^m \\ 1 & s_3 & s_3^2 & \ldots & s_3^n & -z_3 s_3 & -z_3 s_3^2 & \ldots & -z_3 s_3^m \\ \vdots & \vdots & \vdots & \ldots & \vdots & \vdots & \vdots & \ldots & \vdots \\ 1 & s_k & s_k^2 & \ldots & s_k^n & -z_k s_k & -z_k s_k^2 & \ldots & -z_k s_k^m \end{bmatrix} \cdot \begin{bmatrix} a_0 \\ a_1 \\ a_2 \\ \vdots \\ a_n \\ \vdots \\ b_0 \\ b_1 \\ \vdots \\ b_m \end{bmatrix} \quad (18)$$

This way, equation 18 can be presented in matrix notation as follows in equation 19, and therefore characterized as a state estimation problem [45]:

$$z = H_z x \quad (19)$$

To solve the state estimation problem, a number of methods can be applied. Here, the focus resides in the use of an array of Least-Squares algorithms.

A. LEAST SQUARES-BASED METHODS

The conventional Least Squares - LS algorithm aims to find the vector $\hat{x}$ that minimizes $J(\hat{x})$, defined in equation 20 [46].

$$J(\hat{x}) = (z - H_z \hat{x}_k)'(z - H_z \hat{x}_k), \quad (20)$$

where X' represents the transposed matrix of a generic rectangular matrix X.

When the first optimally condition is imposed, the best estimation of $\hat{x}$ can be found through a single non-iterative step given by equation 21 [46].

$$(H_z' H_z \hat{x}) = H_z' z \quad (21)$$

Although the LS method shows to be robust in several applications, a variation of the conventional algorithm can be applied, where a QR decomposition is used and the H_z can be described as a function of the product of two matrices QR, according to equation 22 [47]:

$$H_z = QR \quad (22)$$

Another well-established LS method is the *Weighted Least Squares* - WLS. In this method, weights are attributed to each measurement in order to indicate the most important points during the estimation process [46]. It is similar to the conventional LS method, with a single variation in equation 21, thus, obtaining equation 23 [46].

$$(H_z' W H_z \hat{x}) = H_z' W z \quad (23)$$

The QR decomposition can be also applied to the WLS, with the multiplication of the matrix H and $\hat{x}$ by the weight matrix before the QR factorization (WLS-QR) [47]. As QR decomposition presents itself as a numerically robust alternative to solve the given problem and is one of the fastest and most usual ways to perform the factorization in least-squares algorithms, it was chosen as the method to perform such approximation in the two cases proposed (LS and WLS).

The *Recursive Least Squares* - RLS is another variation of the conventional LS method. It considers that new data can be incorporated into the previous set of measurements, which leads to continuous updating during a dynamic estimation process. This represents an iterative procedure which can be summarized by the following equations [46].

$$\begin{aligned} K_k &= P_{k-1} H_k' (H_k P_{k-1} H_k' + R_k)' \\ \hat{x_k} &= k_1 + K_k(z_k \hat{} - H_k \hat{}_{k-1}) \\ P_k &= (I - K_k H_k) P_{k-1} (I - K_k H_k)' + K_k R_k K_k' \end{aligned} \quad (24)$$

Normally, in the estimation process, the value of P is given by an identity matrix, and the initial value of K is calculated through the first step of equation 24 [46].

B. PROPOSED LS METHOD FOR ESTIMATION PROCESS

The overall proposed estimation process is described in the following steps.

- First, current, voltage, and power measurements are obtained at both ends of the TL for a given range of frequencies. Although the current magnitude can be directly measured, phase values cannot be directly measured, thus the power measurements are used to determine both magnitude and phase values;

- The line parameters are calculated for each frequency point in which values of current, voltage, and power are available (same frequencies of the available reference values 1∼250 Hz obtained through the PSCAD TLCC routine using the Deri-Semlyen method) by the two-port network, representing the required inputs to estimate the curve that represents the frequency-dependent parameters of the line;
- In a second stage, the coefficients a and b of the transfer function in equation 18 are estimated by those five methods presented to obtain the parameter values in the proposed frequency range;
- Finally, the error between the reference values obtained from PSCAD/EMTDC TLCC algorithm with the Deri-Semlyen method, and estimated values, is calculated in order to verify the robustness and eventual limitations of the proposed estimation method.

IV. TESTS AND RESULTS

Tests were performed based on a 400-km overhead TL under several conditions of rated voltage and load, which are described in Table 2. All these scenarios were conducted in separate simulations, being, therefore, uncorrelated. The line characteristics are shown in Figure 2 and extracted from the PSCAD 4.5 database. A transmission line with 400 km length is considered because usually two AC substations are linked by lines with 400 up to 500 km due to voltage stability issues.

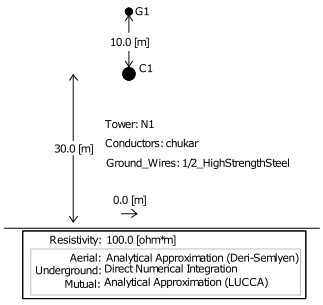

FIGURE 2. Characteristic of the studied overhead TL.

The synchronized measurements were simulated at both line terminals, taking into consideration white gaussian noise of zero mean and signal to noise ratio of 40 and 80 dB, which it was proved an acceptable value in [48].

These measurements are voltage phasors, active and reactive power values, whereas the current phasors are then determined from the power measurements. Regarding the synchronization errors of the double end measurements, a reduction to a minimum value, and therefore almost negligible, is provided when using PMU's or intelligent relays to obtain such measurements, which can be easily considered in cases similar to the ones presented in this paper. As for frequency errors, the standards [49] indicates that they are minimum when working in ranges similar to the ones studied in this paper and with equipment that attend the specified standard levels.

So, in the presence of small measurement errors, the use of traditional LS methods in favour of more complex solutions as total-least squares (TLS) is justifiable, as both presents similar results under such conditions [50]. Then, Five variations of the LS method were tested during the estimation process. The frequency range was limited from 1 Hz up to 250 Hz because most of the switching and maneuver transients are in this range, and also it covers events up to the 4th harmonic as well as oscillatory low-frequency transients [51].

TABLE 2. Test conditions - long line - 400 km.

Case Name	Input Voltage (kV)	R Load Receiving End (Ω)	L Load Receiving End (H)	Load Power (MVA)
Case 1	140	29.4	0.03777	600
Case 2	140	58.8	0.075541	300
Case 3	140	176.4	0.226622	100
Case 4	230	79.35	0.101941	600
Case 5	230	158.7	0.203883	300
Case 6	230	476.1	0.611648	100
Case 7	380	216.6	0.278267	600
Case 8	380	433.2	0.556534	300
Case 9	380	1299	1.669615	100

The load values in Table 2 are calculated based on the technical literature, in which the voltage levels are 140, 230 and 380 kV, and 100, 300 and 600 MVA loads [26]. Some additional tests were also performed for 10 km long line under different values of voltage and load in the same frequency proposed here (1∼250 Hz), with results similar to the ones presented to 400 km line. However, due to the page limitations, and with the intention of focusing in a case more closer to reality, as pointed out in previous sections, only the 400 km line results under the presented conditions were presented.

A. PRELIMINARY ANALYSIS - MEASUREMENT VALIDATION

Figures 3a and 3b show the curves simulated for the cases in Table 2 up to 250 Hz, based on the two-port equations, as introduced in section III. The impedance parameters obtained from measurements and by using the two-port representation are then compared to the reference values calculated by means of the TLCC algorithm with the Deri-Semlyen method available in PSCAD/EMTDC.

It is possible to verify that the calculated frequency-dependent resistance and inductance, respectively, are in accordance with reference values obtained from the TLCC algorithm using Deri-Semlyen method, hereinafter named only as reference values. Some minor variations are observed for cases 2 and 4 at low frequencies around 6 Hz. As these variations are small, limited in number of points and presented only for two of the nine studied cases, they end up not significantly affecting the results under the conditions herein studied as it is seen and easily confirmed by the results presented for all cases, scenarios and algorithms studied. The low influence under such circumstances is also corroborated by the error analysis presented in the following subsections.

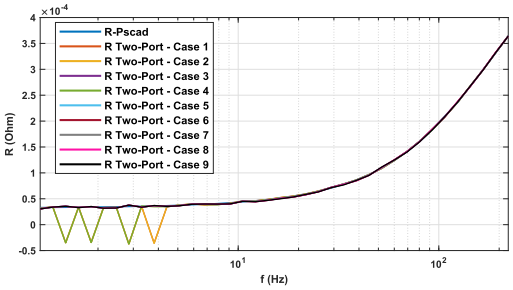

(a) Frequency Dependent Resistance - two-port network vs PSCAD TLCC algorithm with Deri-Semlyen

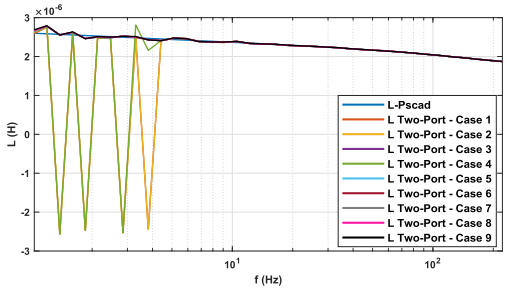

(b) Frequency Dependent Inductance - two-port network vs PSCAD TLCC algorithm with Deri-Semlyen

FIGURE 3. Frequency Dependent Series Parameters - two-port network vs PSCAD TLCC algorithm with Deri-Semlyen.

B. PARAMETERS ESTIMATION

The LS methods are applied to estimate the resistance and inductance from the transfer function in equation 14. A set of reliable measurements are considered to estimate the line parameters in the specified frequency range 1∼250 Hz. The estimation is carried out by fitting the transfer function $Z(s)$ as a third- and seventh-degree polynomial, where the numerator and denominator are indicated by terms n and m, respectively. The conventional LS method, WLS, WLS-QR, RLS and RLS-QR (section III) are denominated in the following analyzes as *algorithms 1 - 5*, respectively.

For this, three types of measurements were used, one considering single measurements, taken in the 15 second instant, for each frequency point in a steady condition (named Single), one considering the last 1000 points of measurements (named Complete), taken between 14.75 seconds and 15 seconds with the established delta. The same 1000 points were also corrupted with white gaussian noise of zero mean and signal to noise ratio (SNR) of 40 and 80 dB (Complete - 40dB/80dB). This second analysis is carried out based on line configurations described in Table 2.

Figures 4a and 4b show the resistance and inductance dependent of the frequency, respectively, fitted by a third-degree polynomial ($n = 3$ and $m = 3$) from the reference values. Analogously, Figures 4c and 4d show the resistance and inductance, respectively, considering function $Z(s)$ as a seventh-degree polynomial. The impedance parameters are estimated by using the five algorithms and 38 frequency samples.

Figures 4e, 4f, 4g and 4h show the error between the fitted values with the five algorithms and reference values of resistance and inductance, respectively, with three- and seven-degree polynomial.

The error values for all algorithms are low through the considered frequency range. Some major errors are observed only at low frequencies up to 10 Hz, for three- and seven-degree transfer functions, with all algorithms. Nevertheless, the best estimation results are obtained with the WLS-QR algorithm for 1∼250 Hz when using the WLS-QR algorithm and measurements divided in six, with the first 1/6 and last 1/6 of the measurements weighted with a value of 0.5 and the remaining with a weight of 1 (all empirically defined, based in the previous knowledge that measurements under and above the steady state frequency,i.e. 50 Hz ∼ 60 Hz, tends to less reliable and more difficult to obtain as the frequency increases or decreases). In this context, the H matrix is composed of real values only.

Initially, only results obtained from a three-degree transfer function (as it is the minimum feasible degree) with a minimum quantity of information available for the base case (Case 9) are presented, in order to prove the robustness of the estimation method even with several restrictions in terms of measurements and representation of the transfer function. The results for resistance and inductance in these minimum conditions, using only 14 frequency samples of the 38 available in the interval 1∼250 Hz, are presented in figures 5a to 5h. The percent error between the reference and estimated values found from the five LS algorithms are presented in figures 6a to 6h. Table 3 shows the coefficient values for all tested algorithms under these conditions, considering also measurements without and with 40 and 80dB noise.

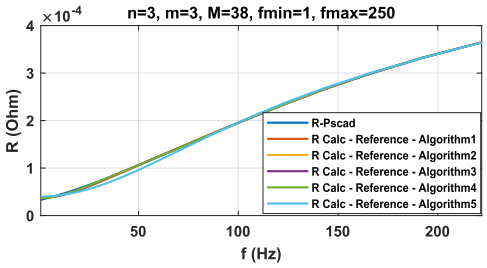

(a) Frequency-dependent resistance.

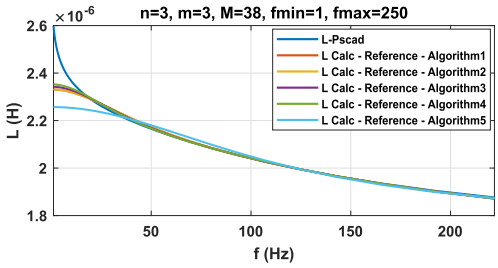

(b) Frequency-dependent inductance.

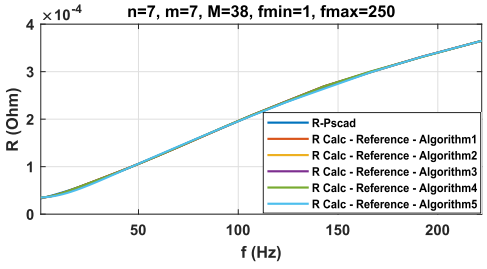

(c) Frequency-dependent resistance.

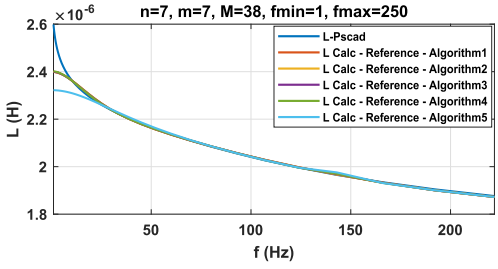

(d) Frequency-dependent inductance.

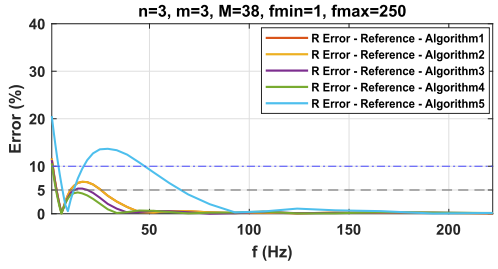

(e) Error between fitting and reference resistance values.

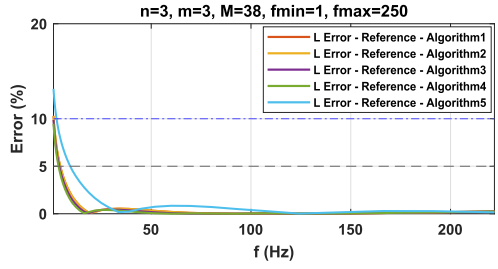

(f) Error between fitting and reference inductance values.

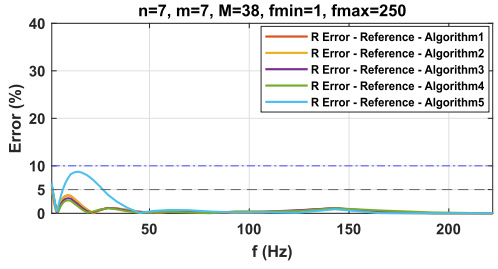

(g) Error between fitting and reference resistance values.

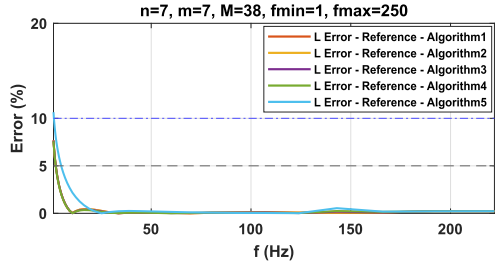

(h) Error between fitting and reference inductance values.

FIGURE 4. **Impedance parameters with five LS methods for 1∼250 Hz.**

From Figures 5a,5c and 5g, it is possible to see a good adherence of the resistance curve to the reference one by using all algorithms when considering single, complete, and 80 dB noisy measurements. In inductance values, all algorithms show minor errors up to 20 Hz.

A deeper error analysis is described in figures 6a to 6h, which shows that using a three-degree transfer function $Z(s)$ with both single and complete measurements in conjunction with WLS-QR, errors are under 5% in the majority of the frequency range of 1∼250 Hz, specifically above 20 Hz for resistance and 10 Hz for inductance. Errors are higher with a 40 dB SNR. When the SNR is 80 dB, results are practically similar to case analyses with complete measurements without noise and single measurements.

The best performance and accuracy were obtained with algorithm 3 WLS-QR, therefore it was tested throughout the same frequency range, based on a three-degree transfer function, for all nine cases defined in Table 2. Figures 7a to 7d show results obtained considering only a single measure without noise. Table 4 shows the coefficients found for these nine studied cases.

It is possible to infer, from Figures 7a and 7b,, that the algorithm shows a good adherence to reference values of resistance and inductance in all cases. In the specific case of the inductance values, the results under 30 Hz, have continued to present a detach from reference values.

Another analysis presented in Figures 7c and 7d shows that loading and supply voltage has a low impact in the

TABLE 3. Coefficient values using the five algorithms with three-degree transfer function (1 Hz ∼ 250 Hz).

Algorithm	a_0	a_1	a_2	a_3	b_1	b_2	b_3
Single Measure							
1	$4.11 \cdot 10^{-5}$	$2.37 \cdot 10^{-6}$	$4.85 \cdot 10^{-9}$	$1.84 \cdot 10^{-12}$	0.00246364	$1.09 \cdot 10^{-6}$	$-3.06 \cdot 10^{-12}$
2	$4.11 \cdot 10^{-5}$	$2.37 \cdot 10^{-6}$	$4.85 \cdot 10^{-9}$	$1.84 \cdot 10^{-12}$	0.00246364	$1.09 \cdot 10^{-6}$	$-3.06 \cdot 10^{-12}$
3	$4.33 \cdot 10^{-5}$	$2.37 \cdot 10^{-6}$	$4.69 \cdot 10^{-9}$	$1.67 \cdot 10^{-12}$	0.00238601	$9.94 \cdot 10^{-7}$	$-6.26 \cdot 10^{-12}$
4	$4.51 \cdot 10^{-5}$	$2.37 \cdot 10^{-6}$	$4.60 \cdot 10^{-9}$	$1.57 \cdot 10^{-12}$	0.00234833	$9.40 \cdot 10^{-7}$	$-8.74 \cdot 10^{-12}$
5	$4.03 \cdot 10^{-5}$	$2.24 \cdot 10^{-6}$	$-7.21 \cdot 10^{-10}$	$-3.18 \cdot 10^{-12}$	$2.61 \cdot 10^{-7}$	$-1.79 \cdot 10^{-6}$	$-2.67 \cdot 10^{-11}$
Complete Measure							
1	$4.29 \cdot 10^{-5}$	$2.40 \cdot 10^{-6}$	$5.40 \cdot 10^{-9}$	$2.00 \cdot 10^{-12}$	0.00271188	$1.20 \cdot 10^{-6}$	$-1.82 \cdot 10^{-11}$
2	$4.29 \cdot 10^{-5}$	$2.40 \cdot 10^{-6}$	$5.40 \cdot 10^{-9}$	$2.00 \cdot 10^{-12}$	0.00271188	$1.20 \cdot 10^{-6}$	$-1.82 \cdot 10^{-11}$
3	$4.47 \cdot 10^{-5}$	$2.39 \cdot 10^{-6}$	$5.22 \cdot 10^{-9}$	$1.86 \cdot 10^{-12}$	0.00263002	$1.12 \cdot 10^{-6}$	$-1.95 \cdot 10^{-11}$
4	$4.62 \cdot 10^{-5}$	$2.38 \cdot 10^{-6}$	$4.98 \cdot 10^{-9}$	$1.65 \cdot 10^{-12}$	0.00251757	$1.00 \cdot 10^{-6}$	$-2.03 \cdot 10^{-11}$
5	$4.78 \cdot 10^{-5}$	$2.24 \cdot 10^{-6}$	$-3.15 \cdot 10^{-10}$	$-2.71 \cdot 10^{-12}$	$1.66 \cdot 10^{-4}$	$-1.52 \cdot 10^{-6}$	$-2.43 \cdot 10^{-11}$
Complete Noisy Measure (40 dB)							
1	$6.44 \cdot 10^{-5}$	$2.08 \cdot 10^{-6}$	$4.74 \cdot 10^{-10}$	$2.07 \cdot 10^{-12}$	0.000334269	$1.04 \cdot 10^{-6}$	$1.20 \cdot 10^{-10}$
2	$6.44 \cdot 10^{-5}$	$2.08 \cdot 10^{-6}$	$4.74 \cdot 10^{-10}$	$2.07 \cdot 10^{-12}$	0.000334269	$1.04 \cdot 10^{-6}$	$1.20 \cdot 10^{-10}$
3	$6.89 \cdot 10^{-5}$	$2.08 \cdot 10^{-6}$	$5.74 \cdot 10^{-10}$	$2.46 \cdot 10^{-12}$	0.000364094	$1.24 \cdot 10^{-6}$	$1.30 \cdot 10^{-10}$
4	$7.30 \cdot 10^{-5}$	$2.08 \cdot 10^{-6}$	$6.56 \cdot 10^{-10}$	$2.94 \cdot 10^{-12}$	0.000382552	$1.48 \cdot 10^{-6}$	$1.46 \cdot 10^{-10}$
5	$6.45 \cdot 10^{-5}$	$2.08 \cdot 10^{-6}$	$4.21 \cdot 10^{-10}$	$2.07 \cdot 10^{-12}$	$3.09 \cdot 10^{-4}$	$1.03 \cdot 10^{-6}$	$1.21 \cdot 10^{-10}$
Complete Noisy Measure (80 dB)							
1	$4.29 \cdot 10^{-5}$	$2.40 \cdot 10^{-6}$	$5.32 \cdot 10^{-9}$	$1.93 \cdot 10^{-12}$	0.00267761	$1.16 \cdot 10^{-6}$	$-1.82 \cdot 10^{-11}$
2	$4.29 \cdot 10^{-5}$	$2.40 \cdot 10^{-6}$	$5.32 \cdot 10^{-9}$	$1.93 \cdot 10^{-12}$	0.00267761	$1.16 \cdot 10^{-6}$	$-1.82 \cdot 10^{-11}$
3	$4.48 \cdot 10^{-5}$	$2.39 \cdot 10^{-6}$	$5.16 \cdot 10^{-9}$	$1.81 \cdot 10^{-12}$	0.00260353	$1.09 \cdot 10^{-6}$	$-1.95 \cdot 10^{-11}$
4	$4.63 \cdot 10^{-5}$	$2.38 \cdot 10^{-6}$	$4.93 \cdot 10^{-9}$	$1.62 \cdot 10^{-12}$	0.00249681	$9.81 \cdot 10^{-7}$	$-2.03 \cdot 10^{-11}$
5	$4.78 \cdot 10^{-5}$	$2.24 \cdot 10^{-6}$	$-3.11 \cdot 10^{-10}$	$-2.70 \cdot 10^{-12}$	$1.68 \cdot 10^{-4}$	-1.52 $\cdot 10^{-6}$	$-2.42 \cdot 10^{-11}$

TABLE 4. Coefficient values (a and b) - all cases - three degree TF - 14 measurements.

Case	a_0	a_1	a_2	a_3	b_1	b_2	b_3
Single Measure - All cases							
1	$4.31 \cdot 10^{-5}$	$2.43 \cdot 10^{-6}$	$6.77 \cdot 10^{-9}$	$3.30 \cdot 10^{-12}$	0.00331378	$1.95 \cdot 10^{-6}$	$-7.35 \cdot 10^{-12}$
2	$4.28 \cdot 10^{-5}$	$2.43 \cdot 10^{-6}$	$6.84 \cdot 10^{-9}$	$3.35 \cdot 10^{-12}$	0.00334559	$1.97 \cdot 10^{-6}$	$-7.35 \cdot 10^{-12}$
3	$4.23 \cdot 10^{-5}$	$2.44 \cdot 10^{-6}$	$7.05 \cdot 10^{-9}$	$3.49 \cdot 10^{-12}$	0.00344347	$2.06 \cdot 10^{-6}$	$-8.53 \cdot 10^{-12}$
4	$4.27 \cdot 10^{-5}$	$2.43 \cdot 10^{-6}$	$6.86 \cdot 10^{-9}$	$3.35 \cdot 10^{-12}$	0.00335425	$1.97 \cdot 10^{-6}$	$-7.68 \cdot 10^{-12}$
5	$4.25 \cdot 10^{-5}$	$2.44 \cdot 10^{-6}$	$6.90 \cdot 10^{-9}$	$3.37 \cdot 10^{-12}$	0.00337672	$1.98 \cdot 10^{-6}$	$-8.81 \cdot 10^{-12}$
6	$4.35 \cdot 10^{-5}$	$2.40 \cdot 10^{-6}$	$5.81 \cdot 10^{-9}$	$2.53 \cdot 10^{-12}$	0.00288641	$1.50 \cdot 10^{-6}$	$-6.71 \cdot 10^{-12}$
7	$4.17 \cdot 10^{-5}$	$2.45 \cdot 10^{-6}$	$7.43 \cdot 10^{-9}$	$3.82 \cdot 10^{-12}$	0.00361022	$2.24 \cdot 10^{-6}$	$-7.09 \cdot 10^{-12}$
8	$4.33 \cdot 10^{-5}$	$2.41 \cdot 10^{-6}$	$6.05 \cdot 10^{-9}$	$2.74 \cdot 10^{-12}$	0.00299648	$1.62 \cdot 10^{-6}$	$-6.28 \cdot 10^{-12}$
9	$4.51 \cdot 10^{-5}$	$2.37 \cdot 10^{-6}$	$4.60 \cdot 10^{-9}$	$1.57 \cdot 10^{-12}$	0.00234833	$9.40 \cdot 10^{-7}$	$-8.74 \cdot 10^{-12}$

estimation process, with only Case 9 presenting a distance of approximately 4% of relative error from the rest of the cases in some points for resistance, and approximately 0.5% from for inductance (both between 10 Hz and 20 Hz). Errors above 5% for resistance values are found only at frequencies lower than 12 Hz. On the other hand, inductance relative error is no more than 1% at the entire frequency range of 1∼250 Hz. In this sense, all cases show to be suitable for estimation both resistance and inductance values.

If WLS-QR is applied considering the same degree three TF, single measurements, but 38 frequency points, the coefficients changes to the ones presented in Table 5. Figures 8a to 8d show the resistance and inductance curves found with these coefficients and the relative errors between the reference values and the estimated ones.

It is possible to see in figures 8a and 8b that the use of the 38 frequency points maintained the adherence of both resistance and inductance curves to the reference values. Again, an in-depth error analysis from figures 8c and 8d shows, in general, little improvement when using such measurements. This improvement is seen especially under 5Hz, with a maximum relative error of 18% for resistance and 9% for inductance, showing that the 14 frequency points end up being enough to maintain a good estimation.

C. POSSIBLE EXTRAPOLATION - DISCUSSION

The simulated range used to get the measurements for all tested cases was set from 1Hz up to 250Hz, for a transmission line with 400 km length. This range covers studies up to the 4th harmonic and some oscillatory transients at low frequencies inside the given frequency range [51]. However, there is a need to extrapolate the values above these frequencies to guarantee a higher range of coverage of transient effects.

When the values of the coefficients found for the WLS-QR algorithm are used to extrapolate the parameter values above the defined range, using a Third-degree transfer function, single measurements, and 14 frequency points, Figures 9a to 9d are established.

It is possible to see from this perspective that the values start to get far from reference values. Even though a good extrapolation (relative error $\leq 5\%$) is obtained until 400 Hz in all cases for resistance values, with faster relative error growth for Case 9. As for the inductance values, an error of no higher than 5% is verified for all cases by considering an

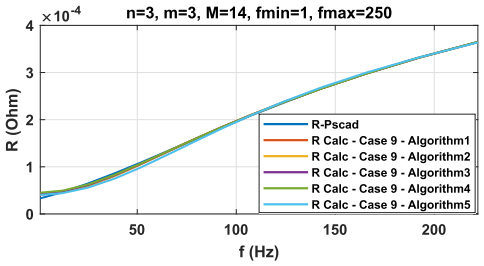

(a) R Estimated x Frequency (Single measure)

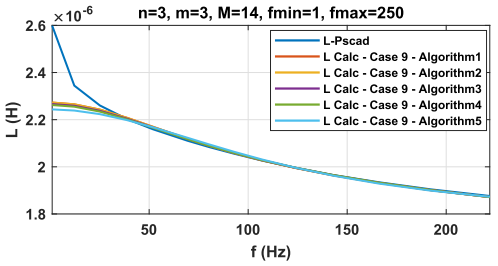

(b) L Estimated x Frequency (Single measure)

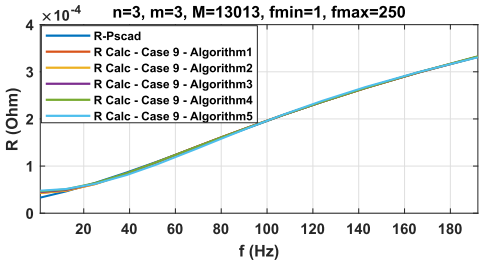

(c) R Estimated x Frequency (Complete measure)

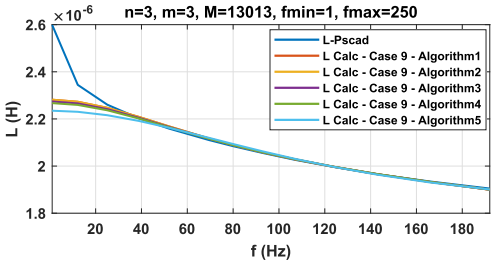

(d) L Estimated x Frequency (Complete measure)

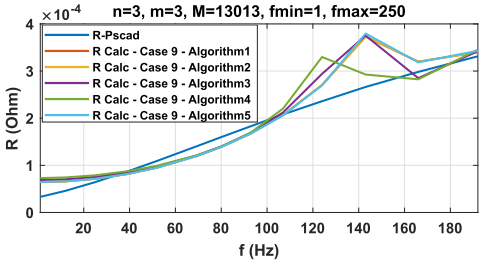

(e) R Estimated x Frequency (Complete measure - 40 dB)

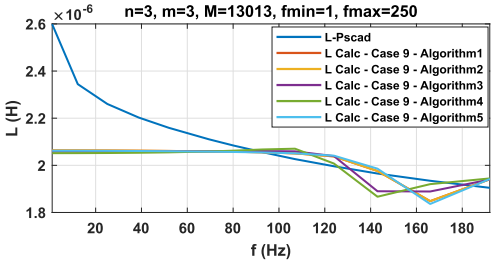

(f) L Estimated x Frequency (Complete measure - 40 dB)

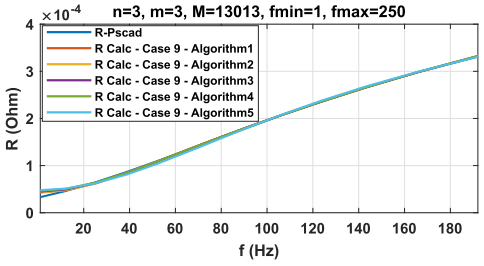

(g) R Estimated x Frequency (Complete measure - 80 dB)

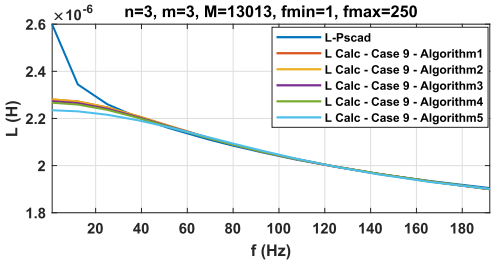

(h) L Estimated x Frequency (Complete measure - 80 dB)

FIGURE 5. **Algorithms Comparison - Estimated Parameters (R and L) x Frequency (1∼250 Hz - degree three TF).**

TABLE 5. **Coefficient values (a and b) - All cases - degree three TF - 38 measurements.**

Case	a_0	a_1	a_2	a_3	b_1	b_2	b_3
Single Measure - All cases							
1	$2.97 \cdot 10^{-5}$	$2.53 \cdot 10^{-6}$	$1.03 \cdot 10^{-8}$	$6.08 \cdot 10^{-12}$	0.00489634	$3.56 \cdot 10^{-6}$	$5.74 \cdot 10^{-12}$
2	$2.95 \cdot 10^{-5}$	$2.52 \cdot 10^{-6}$	$1.02 \cdot 10^{-8}$	$5.98 \cdot 10^{-12}$	0.00485613	$3.50 \cdot 10^{-6}$	$5.68 \cdot 10^{-12}$
3	$3.62 \cdot 10^{-5}$	$2.55 \cdot 10^{-6}$	$1.13 \cdot 10^{-8}$	$6.93 \cdot 10^{-12}$	0.00532535	$4.05 \cdot 10^{-6}$	$-3.00 \cdot 10^{-13}$
4	$3.13 \cdot 10^{-5}$	$2.58 \cdot 10^{-6}$	$1.22 \cdot 10^{-8}$	$7.70 \cdot 10^{-12}$	0.00573351	$4.49 \cdot 10^{-6}$	$7.45 \cdot 10^{-12}$
5	$3.63 \cdot 10^{-5}$	$2.55 \cdot 10^{-6}$	$1.11 \cdot 10^{-8}$	$6.76 \cdot 10^{-12}$	0.00524396	$3.96 \cdot 10^{-6}$	$-8.33 \cdot 10^{-13}$
6	$3.61 \cdot 10^{-5}$	$2.54 \cdot 10^{-6}$	$1.10 \cdot 10^{-8}$	$6.90 \cdot 10^{-12}$	0.00518372	$4.02 \cdot 10^{-6}$	$1.14 \cdot 10^{-11}$
7	$3.61 \cdot 10^{-5}$	$2.56 \cdot 10^{-6}$	$1.15 \cdot 10^{-8}$	$7.25 \cdot 10^{-12}$	0.00544926	$4.23 \cdot 10^{-6}$	$3.00 \cdot 10^{-12}$
8	$3.61 \cdot 10^{-5}$	$2.55 \cdot 10^{-6}$	$1.12 \cdot 10^{-8}$	$7.09 \cdot 10^{-12}$	0.00527436	$4.13 \cdot 10^{-6}$	$1.17 \cdot 10^{-11}$
9	$3.63 \cdot 10^{-5}$	$2.52 \cdot 10^{-6}$	$1.03 \cdot 10^{-8}$	$6.37 \cdot 10^{-12}$	0.00487502	$3.71 \cdot 10^{-6}$	$1.17 \cdot 10^{-11}$

extrapolation up to 3 kHz. So then case 9 presented a higher relative error rate in comparison with the remaining.

When considering a third-degree transfer function, single measurements and 38 frequency points, the extrapolated

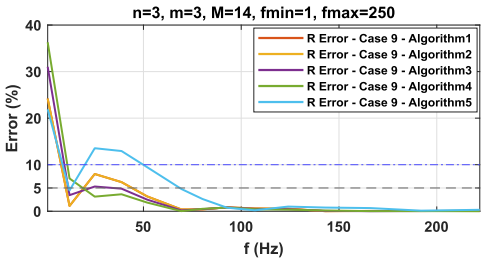

(a) R Relative Error x Frequency (Single measure)

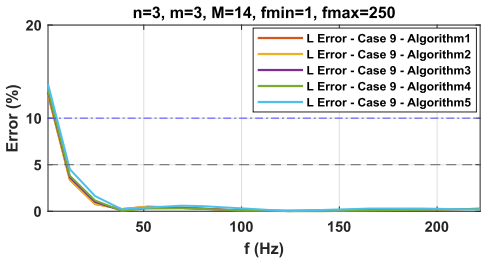

(b) L Relative Error x Frequency (Single measure)

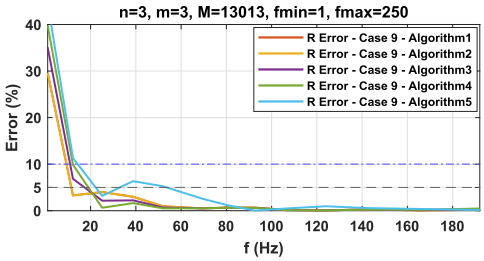

(c) R Relative Error x Frequency (Complete measure)

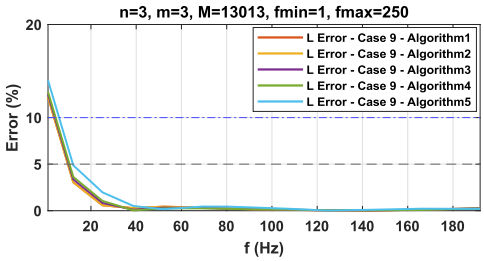

(d) L Relative Error x Frequency (Complete measure)

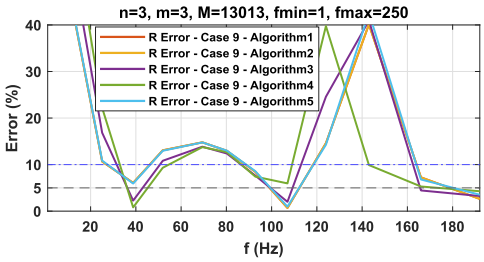

(e) R Relative Error x Frequency (Complete measure - 40 dB)

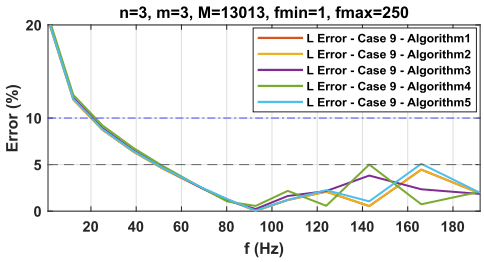

(f) L Relative Error x Frequency (Complete measure - 40 dB)

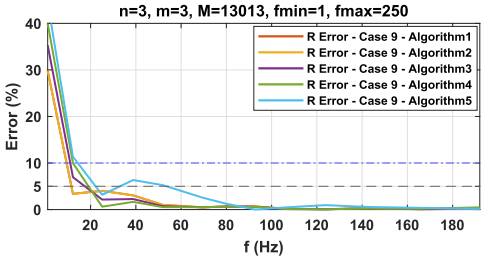

(g) R Relative Error x Frequency (Complete measure - 80 dB)

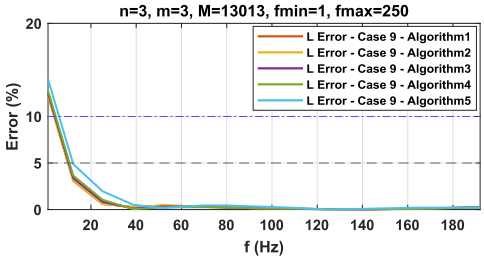

(h) L Relative Error x Frequency (Complete measure - 80 dB)

FIGURE 6. Algorithms Comparison - Estimated Parameters (R and L) Relative Errors (Reference vs Estimated) x Frequency (1∼250 Hz - degree three TF).

estimation and relative error are given through Figures 10a to 10d.

Analyzing the results presented and respective relative error values, it is possible to see that the extrapolation for Cases 6, 8, and 9 stayed near the reference values until 1750 Hz and, for inductance, again in all cases until 3 kHz. The relative error analysis for resistance confirms this, with Cases 6 and 8 staying near a 10% error margin until 2250 Hz, and Case 9 staying under a 10% error margin until 1750 Hz. However, the inductance error alongside the extrapolated margin rose, yet not surpassing 5%.

A test performed with the same 38 frequency points and weight reduced to 0.1, indicates that all Cases stayed under a 10 % relative error margin until 1125 Hz for resistance. Finally, a specific test performed with weight reduced to 0.15 with the range divided in four and the last and first 1/4 of the 38 measurements with this weight, indicates that Cases 6 and 8 stayed near a 5 % relative error margin and Case 9 is maintained under a 5 % relative error margin for an extrapolation until 1125 Hz for resistance, as seen in Figure 11

Thus, such general and conservative analysis of the extrapolation results, the parameter values obtained through the proposal methods presented can be considered as reliable, i.e with a relative error $\leq 5\%$, in the defined range (1∼250 Hz), and up to 400 Hz, near the 7th harmonic (420 Hz), when extrapolating the values to regions without any measurement.

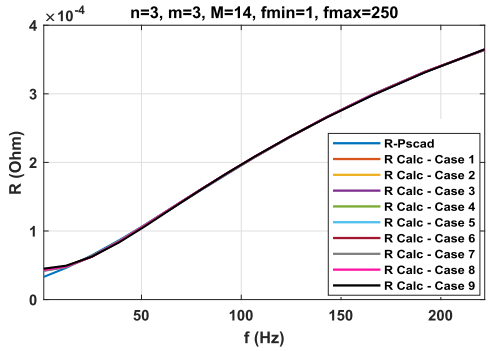

(a) R Estimated x Frequency (Single measure)

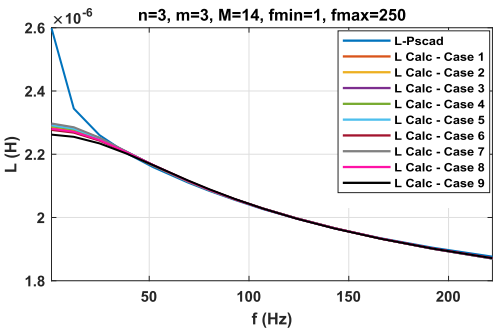

(b) L Estimated x Frequency (Single measure)

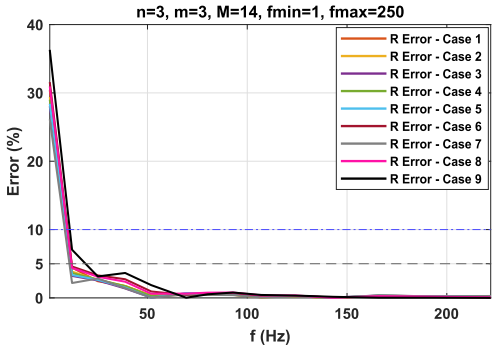

(c) R Relative Error x Frequency (Single measure)

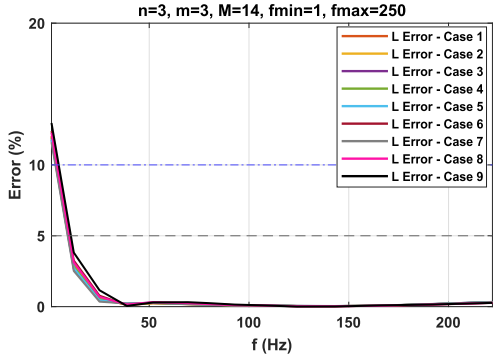

(d) L Relative Error x Frequency (Single measure)

FIGURE 7. **WLS-QR - Estimated Parameters (R and L) and Relative Errors (Reference vs Estimated) x Frequency (1∼250 Hz - three-degree TF for all Cases - 14 points).**

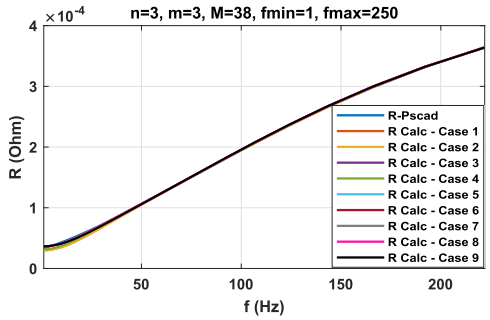

(a) R Estimated x Frequency (Single measure)

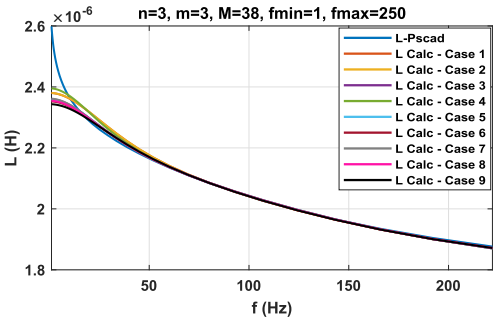

(b) L Estimated x Frequency (Single measure)

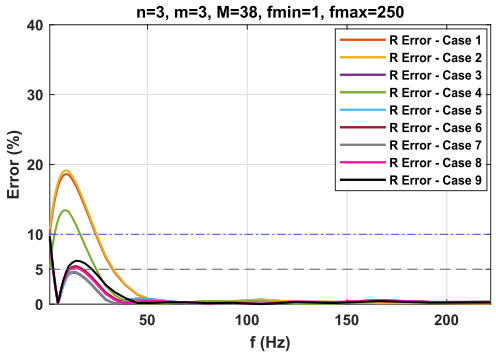

(c) R Relative Error x Frequency (Single measure)

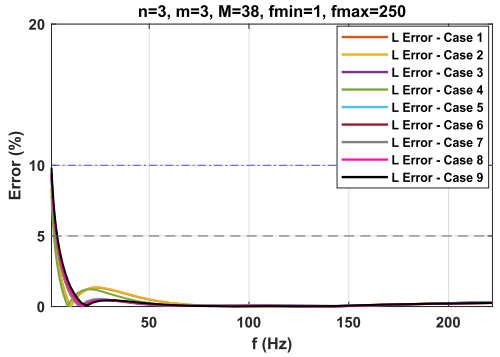

(d) L Relative Error x Frequency (Single measure)

FIGURE 8. **WLS-QR - Estimated Parameters (R and L) and Relative Errors (Reference vs Estimated) x Frequency (1∼250 Hz - degree three TF for all Cases - 38 points).**

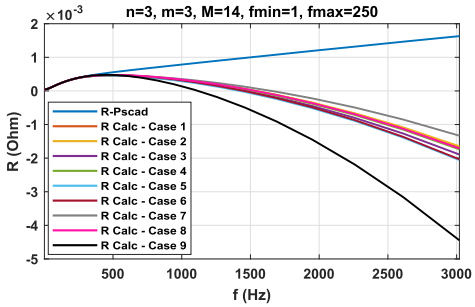

(a) R Extrapolated x Frequency (Single measure - 14 points)

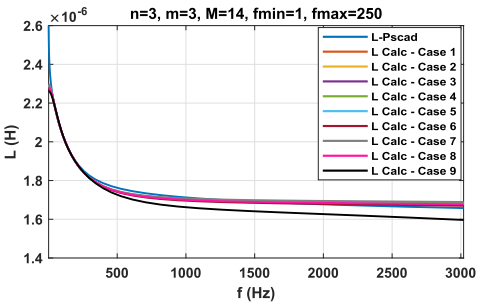

(b) L Extrapolated x Frequency (Single measure - 14 points)

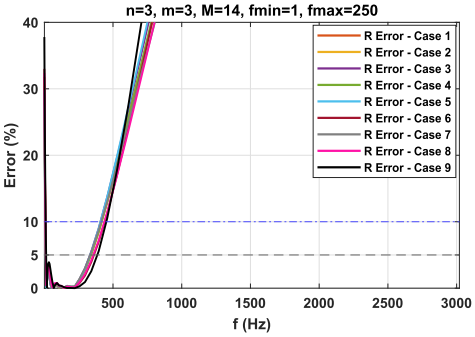

(c) R Extrapolated Error x Frequency (Single measure - 14 points)

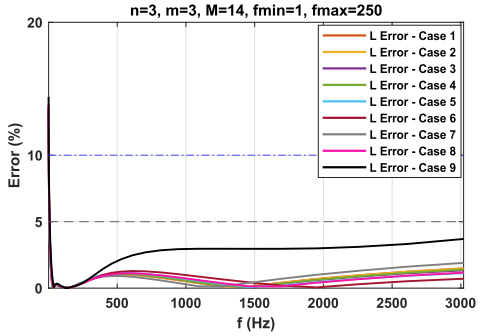

(d) L Extrapolated Error x Frequency (Single measure - 14 points)

FIGURE 9. WLS-QR - Extrapolated Parameters (R and L) and Relative Errors (Reference vs Estimated) x Frequency (degree three TF Single measure - 14 points).

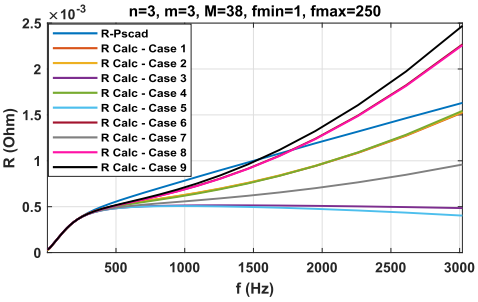

(a) R Extrapolated x Frequency (Single measure - 38 points)

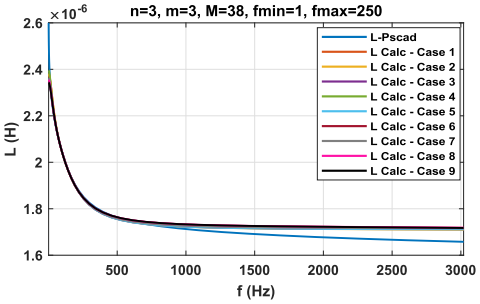

(b) L Extrapolated x Frequency (Single measure - 38 points)

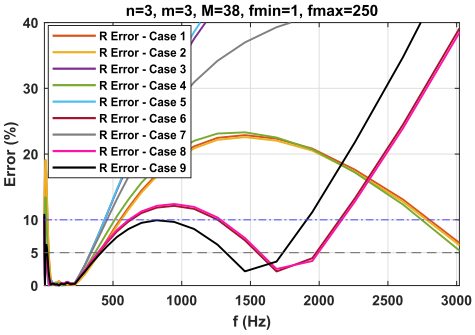

(c) R Extrapolated Error x Frequency (Single measure -38 points)

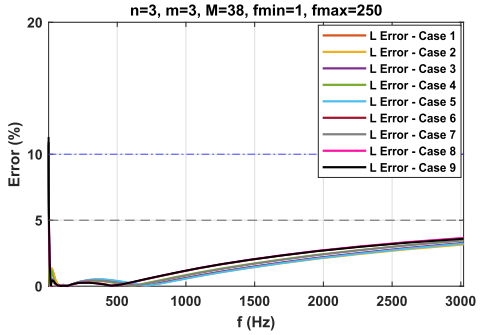

(d) L Extrapolated Error x Frequency (Single measure - 38 points)

FIGURE 10. WLS-QR - Extrapolated Parameters (R and L) and Relative Errors (Reference vs Estimated) x Frequency (degree three TF Single measure - 38 points).

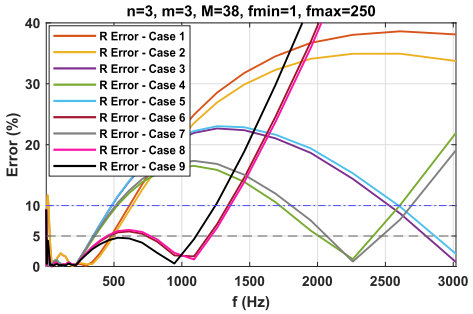

FIGURE 11. R Error between lines (WLS-QR) - Ref. Values x Extrapolated (1∼250 Hz - degree three TF - Single measure - 38 points - Weight 0.15).

V. CONCLUSION

A new method was developed for estimation of frequency-dependent series parameters of long transmission lines based on the impedance fitting by rational function. This technique is usually applied to frequency-dependent line modeling direct in time domain for transient simulations. However, these same fitting techniques applied for parameter estimation represent an original contribution.

First, synchronized measurements are obtained at both terminals of the line. In sequence, impedance parameters are calculated through the two-port model. These values are considered as measurements to estimate the coefficients of frequency-dependent parameters by a transfer function through the Levy method, estimated via five different LS algorithms.

Results proved that parameters can be estimated with good accuracy by the WLS-QR method with a low number of reliable measurements for a frequency range of 1∼250 Hz. With these characteristics, frequency-dependent resistance and inductance are fitted with minor errors. Furthermore, It is possible to extrapolate the values for both resistance and inductance up to 400 Hz, with relative errors ≤ 5 %, even without reliable measurements above 250 Hz. Such reliable measurement can be obtained by means of fault records obtained from digital protective relays, such as previously discussed in the technical literature [39].

Future works aim to use measurements obtained from fault records (i.e. simulating real conditions) and improve the results when dealing with noisy measurements. The second line of research which may be approached consists in improving the extrapolation of results by obtaining measurements above 250 Hz, treating outliers with the replacement of these points, or even applying artificial intelligence and heuristic methods to establish a database of standard lines and guide the reconstruction of the extrapolated region of the curve. Finally, the proposed estimation technique can be extended to non-transposed transmission lines. These further researches are possible from the theory and applications described in this article.

APPENDIX
DERIVED TRANSMISSION LINE EQUATIONS

The two-port network equations presented in section III are derived through the following steps. Considering a long transmission line, the voltage, current and all its distributed parameters can be represented as lumped through the well known corrected (hyperbolic approximations) model, which uses the π model of section III and equations 25, 26, 27 and 28 [43].

$$V_s = V_r \cosh \gamma l + I_r Z_c \sinh \gamma l \tag{25}$$

$$I_s = I_r \cosh \gamma l + \frac{V_r}{Z_c} \sinh \gamma l \tag{26}$$

$$Z_{eq} = Z \frac{\sinh \gamma l}{\gamma l} \tag{27}$$

$$Y_{eq} = Y \frac{\tanh \gamma \frac{l}{2}}{\gamma \frac{l}{2}} \tag{28}$$

Equations 25 to 28 are the fundamental equations of the hyperbolic model. As lines can be represented through a two-port system, the voltage and current equations in the sending end can be expressed through 29 and 30 [43].

$$V_s = AV_r + BI_r \tag{29}$$

$$I_s = CV_r + DI_r \tag{30}$$

Comparing equations 29 and 30 with the fundamental voltage and current equations of the hyperbolic method, it is possible to obtain the values of A, B, C and D parameters of the two-port network, given in equations 31 to 33.

$$A = D = \cosh \gamma l \tag{31}$$

$$B = Z_c \sinh \gamma l \tag{32}$$

$$C = \frac{1}{Z_c} \sinh \gamma l \tag{33}$$

So, to write the two-port parameters in function of voltage and current measurements, as well as the line parameters, presented in equations of section III, the previous equations are taken in consideration with some assumptions. Knowing that $A = D$, equation 31, and that $AD - BC = 1$, this last expression can be written as $A^2 - BC = 1$. Thus, manipulating this last relation leads to equation 34 to find the value of B.

$$B = \frac{A^2 - 1}{C} \tag{34}$$

Replacing B in equation 29 by equation 34, produces equation 35.

$$V_s = AV_r + \frac{A^2 - 1}{C} I_r \tag{35}$$

Through manipulations, equation 35 can be written as equation 36.

$$CV_s = ACV_r + A^2 I_r - I_r \tag{36}$$

As $A = D$, given in equation 31, equation 30 can be represented through equation 37.

$$C = \frac{I_s - I_r A}{V_r} \tag{37}$$

Finally, replacing equation 37 in equation 36 and performing manipulations, leads to equation 7, representing the value

of A as a function of the voltage and current values. The value of equation 10 is the same as equation 7 as $A = D$. Equation 8 is easily achieved manipulating equation 29. Equation 9 is equal to equation 37 when replacing A by D. Now it is possible to use the values of measurements, the two-port parameters A, B, C and D, equations of the hyperbolic approach, the concept of surge impedance of a lossless line and propagation to calculate the values of impedance and admittance of the transmission lines, performed through equations 11 to 13. To derive these last equations, a correlation between the two-port parameters and the hyperbolic approach is needed. When manipulating equation 31 to be represented as $\cos^{-1} A = \gamma l$, it can be later expressed as equation 11. Considering that $\gamma = \sqrt{ZY}$ [43] and replacing the value of γ in equation 11, the latter is represented through equation 13. As for equation 12, its derivation comes from the replacement of Z_c by its value in a lossless line (surge impedance): $Z_c = \sqrt{\frac{Z}{Y}}$ [43]. Solving a system composed by these two latter equations considering the condition established, it is possible to establish the relationship described in equation 12.

REFERENCES

[1] J. J. M. Escobar, O. M. Matamoros, R. T. Padilla, I. L. Reyes, and H. Q. Espinosa, "A comprehensive review on smart grids: Challenges and opportunities," *Sensors*, vol. 21, no. 21, pp. 1–41, 2021.
[2] A. Ghasempour, "Advanced metering infrastructure in smart grid: Requirements, challenges, architectures, technologies, and optimizations," in *Smart Grids: Emerging Technologies, Challenges and Future Directions*, J. Lou, Ed. Nova Science Publishers, 2017, p. 185.
[3] L. Hofmann, "Series expansions for line series impedances considering different specific resistances, magnetic permeabilities, and dielectric permittivities of conductors, air and ground," *IEEE Trans. Power Del.*, vol. 18, no. 2, pp. 564–570, Apr. 2003.
[4] J. H. A. Monteiro, E. Coelho M. Costa, A. J. G. Pinto, S. Kurokawa, O. M. O. Gatous, and J. Pissolato, "Simplified skin-effect formulation for power transmission lines," *IET Sci., Meas. Technol.*, vol. 8, no. 2, pp. 47–53, Mar. 2014.
[5] S. D. Logsdon and D. A. Laird, "Electrical conductivity spectra of smectites as influenced by saturating cation and humidity," *clays clay minerals*, vol. 52, no. 4, pp. 411–420, Aug. 2004.
[6] C. Blattner, "Prediction of soil resistivity and ground rod resistance for deep ground electrodes," *IEEE Trans. Power App. Syst.*, vol. PAS-99, no. 5, pp. 1758–1763, Sep. 1980.
[7] B. Mann and I. Morrison, "Digital calculation of impedance for transmission line protection," *IEEE Trans. Power App. Syst.*, vol. PAS-90, no. 1, pp. 270–279, Jan. 1971.
[8] A. Girgis, "A new Kalman filtering based digital distance relay," *IEEE Trans. Power App. Syst.*, vol. PAS-101, no. 9, pp. 3471–3480, Sep. 1982.
[9] G. Richards and O. Tan, "An accurate fault location estimator for transmission lines," *IEEE Trans. Power App. Syst.*, vol. PAS-101, no. 4, pp. 945–950, Apr. 1982.
[10] C. Fernandez and F. L. Pagola, "Total least squares and discrete-time line models in HV distance protection," *IEEE Trans. Power Del.*, vol. 14, no. 1, pp. 74–79, Jan. 1999.
[11] M. Asprou and E. Kyriakides, "Identification and estimation of erroneous transmission line parameters using PMU measurements," *IEEE Trans. Power Del.*, vol. 32, no. 6, pp. 2510–2519, Dec. 2017.
[12] C. S. Indulkar and K. Ramalingam, "Estimation of transmission line parameters from measurements," *Int. J. Elect. Power Energy Syst.*, vol. 30, no. 5, pp. 337–342, Jun. 2008.
[13] V. Milojević, S. Čalija, G. Rietveld, M. V. Ačanski, and D. Colangelo, "Utilization of PMU measurements for three-phase line parameter estimation in power systems," *IEEE Trans. Instrum. Meas.*, vol. 67, no. 10, pp. 2453–2462, Oct. 2018.
[14] A. Bendjabeur, A. Kouadri, and S. Mekhilef, "Novel technique for transmission line parameters estimation using synchronised sampled data," *IET Gener., Transmiss. Distrib.*, vol. 14, no. 3, pp. 506–515, Feb. 2020.
[15] F. P. Albuquerque, E. C. M. Costa, L. H. B. Liboni, R. F. R. Pereira, and M. C. de Oliveira, "Estimation of transmission line parameters by using two least-squares methods," *IET Gener., Transmiss. Distrib.*, vol. 15, no. 3, pp. 568–575, Feb. 2021.
[16] R. Schulze and P. Schegner, "Parameter identification of unsymmetrical transmission lines," in *Proc. IEEE Bucharest PowerTech*, Jun. 2009, pp. 1–7.
[17] E. C. M. Costa and S. Kurokawa, "Estimation of transmission line parameters using multiple methods," *IET Gener., Transmiss. Distrib.*, vol. 9, no. 16, pp. 2617–2624, 2015.
[18] E. Janecek, P. Hering, P. Janecek, and A. Popelka, "Transmission line identification using PMUs," in *Proc. 10th Int. Conf. Environ. Electr. Eng.*, May 2011, pp. 1–4.
[19] C. Li, Y. Zhang, H. Zhang, Q. Wu, and V. Terzija, "Measurement-based transmission line parameter estimation with adaptive data selection scheme," *IEEE Trans. Smart Grid*, vol. 9, no. 6, pp. 5764–5773, Nov. 2018.
[20] A. S. F. Sobrinho, R. A. Flauzino, L. H. B. Liboni, and E. C. M. Costa, "Proposal of a fuzzy-based PMU for detection and classification of disturbances in power distribution networks," *Int. J. Electr. Power Energy Syst.*, vol. 94, pp. 27–40, Jan. 2018.
[21] L. H. B. Liboni, M. C. de Oliveira, and I. N. D. Silva, "Optimal Kalman estimation of symmetrical sequence components," *IEEE Trans. Instrum. Meas.*, vol. 69, no. 11, pp. 8844–8852, Nov. 2020.
[22] Y. Liao and M. Kezunovic, "Online optimal transmission line parameter estimation for relaying applications," *IEEE Trans. Power Del.*, vol. 24, no. 1, pp. 96–102, Jan. 2009.
[23] T. Segui, P. Bertrand, H. Guillot, P. Hanchin, and P. Bastard, "Fundamental basis for distance relaying with parametrical estimation," *IEEE Trans. Power Del.*, vol. 16, no. 1, pp. 99–104, Jan. 2001.
[24] J. A. Jiang, C.-S. Chen, and C.-W. Liu, "A new protection scheme for fault detection, direction discrimination, classification, and location in transmission lines," *IEEE Trans. Power Del.*, vol. 18, no. 1, pp. 34–42, Jan. 2003.
[25] Y. Du and Y. Liao, "Online estimation of power transmission line parameters, temperature and sag," in *Proc. North Amer. Power Symp.*, Aug. 2011, pp. 1–6.
[26] G. A. Asti, R. C. da Silva, S. Kurokawa, and E. C. M. da Costa, "Identification of transmission line parameters from temporal measurements of currents and voltages in their terminals: Influence oh the length line," in *Proc. IEEE Power Energy Soc. Gen. Meeting*, Jul. 2012, pp. 1–7.
[27] K. Dasgupta and S. A. Soman, "Line parameter estimation using phasor measurements by the total least squares approach," in *Proc. IEEE Power Energy Soc. Gen. Meeting*, Jul. 2013, pp. 1–5.
[28] R. Rubesa, V. Kirincic, and S. Skok, "Transmission line positive sequence impedance estimation based on multiple scans of phasor measurements," in *Proc. IEEE Int. Energy Conf. (ENERGYCON)*, May 2014, pp. 644–651.
[29] S. S. Mousavi-Seyedi, F. Aminifar, and S. Afsharnia, "Application of WAMS and SCADA data to online modeling of series-compensated transmission lines," *IEEE Trans. Smart Grid*, vol. 8, no. 4, pp. 1968–1976, Jul. 2017.
[30] Y. Sun, Z. Gao, S. Hu, H. Sun, A. Su, S. Wang, K. Gao, and W. Ge, "A method of estimating transmission line parameters using cloud computing based on distributed intelligence," in *Proc. IEEE 17th Int. Conf. Cognit. Informat. Cognit. Comput. (ICCI*CC)*, Jul. 2018, pp. 495–500.
[31] S. M. S. Ghiasi, M. Abedi, and S. H. Hosseinian, "Mutually coupled transmission line parameter estimation and voltage profile calculation using one terminal data sampling and virtual black-box," *IEEE Access*, vol. 7, pp. 106805–106812, 2019.
[32] Y. Zhang and Y. Liao, "Kalman filter approach for line parameter estimation for long transmission lines," in *Proc. IEEE Power Energy Conf. Illinois (PECI)*, Feb. 2020, pp. 1–8.
[33] A. Shoukat, M. A. Mughal, and A. Hussain, "Short transmission line parameter estimation using firefly algorithm," in *Proc. Int. Conf. Emerg. Power Technol. (ICEPT)*, Apr. 2021, pp. 1–5.
[34] W. S. Hassanein, M. M. Ahmed, M. I. Mosaad, and A. Abu-Siada, "Estimation of transmission line parameters using voltage-current measurements and whale optimization algorithm," *Energies*, vol. 14, no. 11, p. 3239, Jun. 2021, doi: 10.3390/en14113239.
[35] M. S. Sarto, A. Scarlatti, and C. L. Holloway, "On the use of fitting models for the time-domain analysis of problems with frequency-dependent parameters," in *Proc. IEEE EMC Int. Symp. Symp. Rec. Int. Symp. Electromagn. Compat.*, Aug. 2001, pp. 588–593.

[36] A. St. Leger, V. Cecchi, M. Basu, K. Miu, and C. Nwankpa, "Automated system for determining frequency dependent parameter model of transmission line in a laboratory environment," *Measurement*, vol. 92, pp. 1–10, Oct. 2016, doi: 10.1016/j.measurement.2016.05.064.
[37] S. Bogarra, J.-R. Riba, V. Sala-Caselles, and A. Garcia, "Optimal fitting of high-frequency cable model parameters by applying evolutionary algorithms," *Int. J. Electr. Power Energy Syst.*, vol. 87, pp. 16–26, May 2017, doi: 10.1016/j.ijepes.2016.11.006.
[38] S. Kurokawa, F. N. R. Yamanaka, A. J. Prado, and J. Pissolato, "Inclusion of the frequency effect in the lumped parameters transmission line model: State space formulation," *Electr. Power Syst. Res.*, vol. 79, no. 7, pp. 1155–1163, Jul. 2009.
[39] R. Schulze, P. Schegner, and R. Živanović, "Parameter identification of unsymmetrical transmission lines using fault records obtained from protective relays," *IEEE Trans. Power Del.*, vol. 26, no. 2, pp. 1265–1272, Apr. 2011.
[40] A. Deri, G. Tevan, A. Semlyen, and A. Castanheira, "The complex ground return plane a simplified model for homogeneous and multilayer Earth return," *IEEE Trans. Power App. Syst.*, vol. PAS-100, no. 8, pp. 3686–3693, Aug. 1981.
[41] B. Gustavsen and A. Semlyen, "Simulation of transmission line transients using vector fitting and modal decomposition," *IEEE Trans. Power Del.*, vol. 13, no. 2, pp. 605–614, Apr. 1998.
[42] A. J. G. Pinto, E. C. M. Costa, S. Kurokawa, J. H. A. Monteiro, J. L. de Franco, and J. Pissolato, "Analysis of the electrical characteristics and surge protection of EHV transmission lines supported by tall towers," *Int. J. Electr. Power Energy Syst.*, vol. 57, pp. 358–365, May 2014.
[43] W. H. Stevenson and J. Grainger, *Power System Analysis*, 1st ed. New York, NY, USA: McGraw-Hill, 1994.
[44] E. S. Banuelos-Cabral, J. A. Gutierrez-Robles, and B. Gustavsen, Eds., *Rational Fitting Techniques for the Modeling of Electric Power Components and Systems Using MATLAB Environment*. London, U.K.: IntechOpen, 2017. [Online]. Available: https://www.intechopen.com/books/6624, doi: 10.5772/intechopen.71692.
[45] A. Abur and A. G. Exposito, *Power System State Estimation: Theory Implementation*, 1st ed. New York, NY, USA: Marcel Dekker, 2004. [Online]. Available: http://www.crcpress.com/product/isbn/9780824755706
[46] D. Simon, *Optimal State Estimation: Kalman, H, Nonlinear Approaches*. Hoboken, NJ, USA: Wiley, 2006.
[47] G. H. Golub and C. F. Van Loan, "Matrix computations," in *Johns Hopkins Studies in the Mathematical Sciences*. Baltimore, MD, USA: Johns Hopkins Univ. Press, 2013.
[48] M. Brown, M. Biswal, S. Brahma, S. J. Ranade, and H. Cao, "Characterizing and quantifying noise in PMU data," in *Proc. IEEE Power Energy Soc. Gen. Meeting (PESGM)*, Jul. 2016, pp. 1–5.
[49] *IEEE/IEC International Standard Measuring Relays and Protection Equipment—Part 118-1: Synchrophasor for Power Systems Measurements*, Standard IEC/IEEE 60255-118-1:2018, 2018, pp. 1–78.
[50] S. Van Huffel and J. Vandewalle, "On the accuracy of total least squares and least squares techniques in the presence of errors on all data," *Automatica*, vol. 25, no. 5, pp. 765–769, Sep. 1989. [Online]. Available: https://www.sciencedirect.com/science/article/pii/0005109889900332
[51] J. A. Martinez-Velasco, *Power System Transients: Parameter Determination*, 1st ed. Boca Raton, FL, USA: CRC Press, 2010.

CASSIO GEREZ received the B.S. degree in electrical engineering (electronics) from the Escola de Engenharia de Lins (EEL), Unilins, in 2009, and the M.S. degree in electrical engineering from the Federal University of ABC (UFABC), in 2017. He is currently pursuing the Ph.D. degree in electrical engineering with the University of São Paulo (USP). His research interests include electrical energy distribution and transmission systems, parameter estimation, computational modeling applied to electrical power systems, and optimization.

EDUARDO WERLEY S. ÂNGELOS (Member, IEEE) received the Ph.D. degree in electrical engineering from the University of Sao Paulo, Sao Carlos, Brazil, in 2013. He was a Visiting Scholar with the Electrical and Computer Engineering Department, Northeastern University, Boston, in 2015. He was a Visiting Professor with the Federal University of ABC, Santo André, Brazil, in 2019 and 2020. He is currently a Collaborator with the Research, Innovation and Dissemination Center for Neuromathematics (NeuroMat), USP.

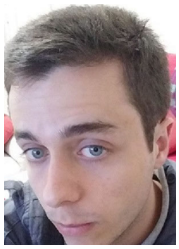

FELIPE P. ALBUQUERQUE received the B.S. and M.S. degrees in electrical engineering from the University of São Paulo (USP), São Paulo, in 2019 and 2021, respectively. He is currently pursuing the Ph.D. degree in electrical engineering with the University of São Paulo (USP). His research interests include computational analysis and modeling of electric components, extra-high voltage transmission systems, transmission line parameter estimation through system identification methods, and stochastic modeling of noise in electric measurements.

EDUARDO C. MARQUES DA COSTA received the Ph.D. degree in electrical engineering from the University of Campinas (UNICAMP), Campinas, Brazil, in 2013. He is currently an Assistant Professor with the Polytechnic School, University of São Paulo. His research interests include power transmission systems, electromagnetic transients, power system modeling, and identification methods.

ALFEU J. SGUAREZI FILHO (Senior Member, IEEE) received the Ph.D. degree from Campinas University, Brazil, in 2010. He is currently a Professor with the Federal University of ABC (UFABC), Santo André, Brazil, where he is teaching in the areas of electrical machines, power electronics, and electrical drives. His research interests include machine drives, wind and photovoltaic energies, and electrical power systems.

LUISA H. BARTOCCI LIBONI (Member, IEEE) received the B.S. and Ph.D. degrees in electrical engineering from the University of São Paulo (USP), Sertãozinho, in 2010 and 2017, respectively. She has a major in education from the Federal Institute of Education, Science, and Technology of São Paulo (IFSP), Brazil, in 2011. She was a Visiting Ph.D. Scholar with the Department of Mechanical and Aerospace Engineering, University of California at San Diego (UCSD), San Diego, CA, USA. She is currently an Associate Professor with the Department of Electrical and Computer Engineering, IFSP; and a Senior Researcher with the Department of Electrical and Computer Engineering, USP. Her research interests include state estimation, optimization, dynamic systems, machine learning, and smart grids.